Detection of uncompensated magnetization at the interface of an epitaxial antiferromagnetic insulator

Pavel N. Lapa,[1] Min-Han Lee,[1, 2] Igor V. Roshchin,[3] Kirill D. Belashchenko[4] and Ivan K. Schuller[1]

[1]*Department of Physics, University of California, San Diego, La Jolla, California 92093, USA*

[2]*Materials Science and Engineering Program, University of California San Diego, La Jolla, California 92093, USA*

[3]*Department of Material Science and Engineering, Texas A&M University, College Station, Texas 77843-4242, USA*

[4]*Department of Physics and Astronomy and Nebraska Center of Materials and Nanoscience, University of Nebraska–Lincoln, Lincoln, Nebraska 68588-0299, USA*

We have probed directly the temperature and magnetic field dependence of pinned uncompensated magnetization at the interface of antiferromagnetic FeF_2 with Cu, using FeF_2-Cu-Co spin valves. Electrons polarized by the Co layer are scattered by the pinned uncompensated moments at the FeF_2-Cu interface giving rise to giant magnetoresistance. We determined the direction and magnitude of the pinned uncompensated magnetization at different magnetic fields and temperatures using the angular dependences of resistance. The strong FeF_2 anisotropy pins the uncompensated magnetization along the easy axis independent of the cooling field orientation. Most interestingly, magnetic fields as high as 90 kOe, cannot break the pinning at the FeF_2-Cu interface. This proves that the pinned interfacial magnetization is strongly coupled to the antiferromagnetic order inside the bulk FeF_2 layer. Studies as a function of FeF_2 crystalline orientation show that uncompensated spins are only detected in a spin valve with (110) crystal orientation, but not in valves containing FeF_2(100) and FeF_2(001). This observation is in agreement with symmetry-related considerations which predict the equilibrium boundary magnetization for the FeF_2(110) layer.

I. INTRODUCTION

Antiferromagnets are essential for the development of spintronics applications [1]. They display faster dynamics than ferromagnets, which can be exploited in devices operating at terahertz frequencies [2,3]. Vanishing macroscopic magnetization eliminates stray fields, making antiferromagnetic devices insensitive to external magnetic fields. The major drawback is that the antiferromagnetic order cannot be easily manipulated nor detected using commonly available techniques. Moreover, laboratory magnetic fields can only affect uncompensated magnetic moments present due to defects.

However, local compensation of magnetic moments in bulk antiferromagnets may not be preserved at an interface either for symmetry reasons or because of imperfections. Moreover, the magnetic moment magnitude and orientation at interfaces may vary significantly depending on the crystalline orientation of the antiferromagnetic layer [4]. For certain orientations of an antiferromagnetic layer, the interfacial spin structure may be uncompensated, enabling useful functionality in magnetic heterostructures. For example, pinning of the uncompensated interfacial magnetization is responsible for exchange bias in

ferromagnet/antiferromagnet heterostructures [4-10]. Additionally, giant and tunneling magnetoresistance, extensively studied in ferromagnetic spin valves, may exhibit new properties when ferromagnets are substituted by antiferromagnets [11,12]. Low spin accumulation at interfaces with antiferromagnets may be a hindrance for the development of antiferromagnetic spin valves for practical applications. However, they may provide crucial information on the interfacial uncompensated spin configuration. This information is necessary for further development of antiferromagnetic spintronics and is difficult to obtain by other experimental techniques.

Crucial insight into the surface magnetism of antiferromagnets can be inferred from symmetry considerations. A single-domain antiferromagnet, without time-reversal symmetry in its magnetic point group, has an uncompensated magnetization at a generically oriented surface, which is thermodynamically stable and protected against surface roughness [13,14]. The lack of macroscopic time-reversal symmetry in an antiferromagnet is associated with linear or nonlinear magnetoelectricity [15]. In particular, it was demonstrated that the boundary magnetization of a linear magnetoelectric can be switched by a combination of external electric and magnetic fields [14,16]. The linear magnetoelectric effect is forbidden by inversion symmetry in transition-metal fluorides with the rutile lattice, such as FeF_2, but a time-reversal-breaking single-domain state can still be achieved by direct coupling of the boundary magnetization to an external magnetic field.

In this paper, we use antiferromagnet-ferromagnet spin valves (AFSV) [11] to study the uncompensated magnetization and its pinning at the surface of differently oriented antiferromagnetic FeF_2 layers. The valves consist of an epitaxially grown FeF_2 layer and a ferromagnetic Co layer separated by a thin Cu spacer. The purpose of these spin valves is to detect giant magnetoresistance (GMR) which depends on the mutual orientation of the magnetizations in the Co layer and at the FeF_2-Cu interface [Fig. 1(a)]. In this context, the most useful aspect of FeF_2 is that it is an insulating antiferromagnet, therefore, only the FeF_2-Cu interface is accessible to free charge carriers in an AFSV. Because of this certain features of the magnetoresistance may be directly attributed to the uncompensated magnetization at this interface.

Antiferromagnetic insulators are of interest due to their possible applications in low-power magnonic devices [17,18]. FeF_2 is a well-studied antiferromagnet with a tetragonal rutile structure and simple Néel spin ordering. Below the Néel temperature (78 K), the strong magnetic anisotropy provides high stability of this spin structure along the easy, *c* axis ([001] direction). As discussed below, symmetry considerations show that the (110) surface of FeF_2 has a thermodynamically stable macroscopic uncompensated magnetization, whereas (001) and (100) surfaces do not. This feature is consistent with the fact that the magnitude of the exchange bias in FeF_2/ferromagnet systems strongly depends on the FeF_2 crystallographic orientation [4]. Although the interfacial magnetization is much lower than that in the Co layer, the AFSV technique enabled us to detect and

study its behavior in a wide range of temperatures and magnetic fields. Specifically, the measurements reveal some peculiar properties of the interfacial magnetization which are distinctively different from its ferromagnetic counterpart: the interfacial magnetization exhibits unprecedented stability, and magnetization reversal can only be observed at temperatures close to the Néel temperature.

II. EXPERIMENTAL DETAILS

FeF_2(30 nm)/Cu(10 nm)/Co(5 nm)/Ti(5 nm) AFSV were grown using electron beam gun evaporation on MgF_2 (110), MgF_2 (100), and MgF_2 (001) single-crystal substrates. The FeF_2 layer was grown at 300ºC at a rate of 0.3 Å/sec. To avoid interdiffusion, the rest of the layers (Cu, Co, Ti) were grown at a rate of 0.5 Å/sec after the substrates were cooled down to 50ºC. MgF_2 and FeF_2 have closely matching crystallographic structures and lattice parameters which allows for epitaxial growth of FeF_2(110), FeF_2(100), and FeF_2(001) on the MgF_2 substrates. The corresponding AFSVs are denoted as FeF_2(110)/Cu/Co, FeF_2(100)/Cu/Co and FeF_2(001)/Cu/Co further in the text.

Four probe electrical resistivity measurements were performed on 8 mm × 2 mm stripes with the current injected along the long edge. For the FeF_2(110)/Cu/Co and FeF_2(100)/Cu/Co AFSVs, the FeF_2 [001] easy axis is perpendicular to the long edge of the stripes. The spin valves were installed on a horizontal rotator, i.e., with the external magnetic field in the plane of the film. The angular orientation of AFSVs is defined by the angle, θ, between the FeF_2 [001] easy axis and the positive magnetic-field direction [Fig. 1(b)]. Thus, 0º corresponds to the orientation in which the magnetic field is perpendicular to the long edge of the stripes and parallel to the FeF_2 easy axis [Fig. 1(b)]. Whereas the results presented in this paper are based on one set of AFSVs, two additional sets of AFSVs confirmed the reproducibility of these results.

III. EXPERIMENTAL RESULTS

To get an insight into pinning processes emerging at the FeF_2-Cu interface, the following measurement protocol was used. An AFSV was cooled from 300 K to a temperature T in a magnetic field H_{cool} while the valve was oriented at θ_{cool}. The resistance R was then measured as a function of the sample orientation in magnetic field H_{meas} while θ was varied from 0º to 360º and back to 0º. The angular dependences of the resistance for a FeF_2(110)/Cu/Co AFSV measured after cooling in a 90-kOe magnetic field applied along the easy axis (θ_{cool} = 0º) and after cooling in zero magnetic field (ZFC) are shown in Fig. 1(c) and Fig. 1(d), respectively. The measurements were conducted at 10 K in the H_{meas} = 90 kOe magnetic field. Both curves exhibit a harmonic behavior as expected due to anisotropic magnetoresistance (AMR). However, there is a salient feature that cannot be explained by AMR. The curve for the field-cooled AFSV [Fig. 1(c)] is not symmetric under reversal of the magnetic field along the cooling direction: resistance at θ = 0º is about 3 mΩ higher than at 180º, whereas it is the same at θ = 90º and 270º. On the

other hand, the resistance of the ZFC sample is symmetric under field reversal [Fig. 1(d)]. The overall vertical shift of the curves in Fig. 1(c) and Fig. 1(d) occurs because a lock-in detector got reconfigured between the corresponding measurements. If the cooling magnetic field is reversed (θ_{cool} = 180º), the global minimum of the resistance is observed at 0º instead of 180º, and the resistance at θ = 180º is 3 mΩ higher. These observations clearly indicate that the cooling field yields a preferred orientation that enhances carrier scattering.

Overall, the angular dependence of the resistance can be described as

$$R(\theta) = R_0 + \Delta R_{AMR} \sin^2(\theta) + \Delta R_{GMR} \sin^2((\theta - \theta_{pin})/2), \qquad (1)$$

where R_0 is the resistance of the valve in zero magnetic field, and the second term describes the contribution from AMR. The third term describes a GMR contribution caused by spin-dependent scattering on a magnetization pinned at θ_{pin} after field-cooling. The fit of the experimental data to Eq. (1) with three adjustable parameters ΔR_{AMR}, ΔR_{GMR}, and θ_{pin} is shown by thin grey lines in Fig. 1(c) and Fig. 1(d). For cooling along the easy axis (θ_{cool} = 0º and 180º), fitting yields $\theta_{pin} = \theta_{cool}$ + 180º.

The temperature dependence of the normalized GMR ($\Delta R_{GMR}/R_0$) for the FeF_2(110)/Cu/Co AFSV is shown in Fig. 2. ΔR_{GMR} values are obtained by fitting to Eq. (1) angular dependences of the resistance measured in the 90-kOe magnetic field at a sequence of increasing temperatures. Prior to the measurements, the AFSV was cooled to 10 K in the 90-kOe magnetic field applied along the easy axis of FeF_2. The GMR decreases monotonically with increasing temperature up to 60 K and then sharply drops to zero.

Fig. 3(a) shows the dependences of $\Delta R_{GMR}/R_0$ on H_{meas} at 10 K (squares), 65 K (circles) and 70 K (stars). For these measurements, the FeF_2(110)/Cu/Co valve was first cooled to the "target temperature" in the 90-kOe magnetic field applied along the easy axis (θ_{cool} = 0º). Then, the magnetic field was decreased to 5 kOe, and the angular dependence of the resistance was measured in H_{meas} which was gradually increased from 5 kOe to 90 kOe and then decreased back to 5 kOe. The H_{meas}-up and H_{meas}-down branches of the curves are shown in red and blue colors, respectively. The AFSV was kept at θ_{cool} while H_{meas} was varied. Fig. 3(a) shows that the GMR at 10 K remains constant for all H_{meas}. At the same time, GMR signal measured at 65 and 70 K becomes almost zero in high magnetic fields. Thus, the GMR signal at 65 K is significantly suppressed if H_{meas} is above 80 kOe. An increase in temperature by 5 K causes a significant reduction in the suppression field: the GMR signal at 70 K disappears if H_{meas} is above 55 kOe.

The angular dependence of the resistance for the FeF_2(110)/Cu/Co AFSV was measured at 70 K in a 10-kOe magnetic field after three different protocols: (1) cooling in a 90-kOe magnetic field at θ_{cool} = 0º and decreasing the field to 10 kOe while

the valve is at 0º [Fig. 3(b)]; (2) after completing the first measurement, rotating the AFSV 180º, applying a 50-kOe magnetic field (which is thus opposite to the cooling field), and measuring at the same 10-kOe magnetic field [Fig. 3(c)]; and (3) after completing the second measurement, applying a larger 70-kOe magnetic field (again opposite to the cooling field) prior to the measurement at 10 kOe [Fig. 3(d)]. Fig. 3(b) and Fig. 3(c) show that the resistance at 180º is about 1.2 mΩ lower compared to that at 0º, $\theta_{pin} = \theta_{cool} + 180º = 180º$. At the same time, after applying the 70-kOe in the direction which is opposite to the cooling field, the resistance becomes about 1 mΩ higher at 180º compared to that at 0º.

All the data for the FeF_2(110)/Cu/Co AFSV presented so far were obtained after cooling the valve in a magnetic field applied along the easy axis of FeF_2 ($\theta_{cool} = 0º$). Fig. 4(a) shows the angular dependence of the resistance measured at 10 K in a 90-kOe magnetic field after cooling the same AFSV in a 90-kOe field applied perpendicular to the easy axis ($\theta_{cool} = 90º$). The angular dependence is similar to the one at $\theta_{cool} = 0º$ [Fig. 1(c)]: in both curves, the resistance at $\theta = 180º$ is lower than at 0º, whereas those at 90º and 270º are the same. The only difference between the curves obtained at $\theta_{cool} = 0º$ [Fig. 1(c)] and $\theta_{cool} = 90º$ [Fig. 4(a)] is that the GMR (ΔR_{GMR}) is slightly lower for the latter curve (3 mΩ vs 2.6 mΩ). For $\theta_{cool} = 270º$ (not shown), the resistance at 180º becomes higher than the resistance at 0º, and the resistances at 90º and 270º remains the same. The fits of the data to Eq. (1) yield θ_{pin} is 180º and 0º for $\theta_{cool} = 90º$ and $\theta_{cool} = 270º$, respectively.

Further measurements reveal that as θ_{cool} is increased slightly above 90º, θ_{pin} experiences an abrupt change by 180º. This is inferred from the angular dependences of the resistance measured after cooling the valve in 90-kOe at $\theta_{cool} = 70º$ [Fig. 4(b)] and $\theta_{cool} = 110º$ [Fig. 4(c)]. The resistance asymmetry along the easy axis implies that $\theta_{pin} = 180º$ after the 70º cooling and $\theta_{pin} = 0º$ after the 110º cooling. Thus, θ_{pin} switches by 180º when the cooling angle is $90º < \theta_{cool} < 110º$.

The same measurement protocols as were used for the FeF_2(110)/Cu/Co valve, were applied to the FeF_2(100)/Cu/Co and FeF_2(001)/Cu/Co AFSVs. No GMR signal was detected for these AFSVs. Since the easy [001] axis is perpendicular to the FeF_2(001)/Cu/Co valve's plane, this valve was also installed on a vertical rotator, and a number of $R(\theta)$ curves were measured in a 90-kOe magnetic field rotated out of plane. The 90-kOe magnetic field is sufficiently strong to overcome the shape anisotropy of the Co layer, ensuring that the Co layer still behaves like a free layer and its magnetization rotates out of plane in unison with the external magnetic field. No GMR signal was detected for these out-of-plane measurements of the FeF_2(001)/Cu/Co AFSV.

IV. DISCUSSION

A. Origin of GMR in the FeF_2/Cu/Co valve

The central experimental result is that the resistance of the FeF_2(110)/Cu/Co AFSV acquires a GMR-like contribution when the valve is field-cooled below the Néel temperature of FeF_2 [Fig. 1(c)]. We developed a model which explains the origin of this GMR signal and describes the magnetization processes occurring in FeF_2 antiferromagnet at different temperatures and magnetic fields. A crucial assumption of the model is that cooling in a field only influences the insulating FeF_2. Therefore, the change in the magnetoresistance for different cooling procedures can only be related to the magnetization processes at the FeF_2-Cu interface. The model assumes that the uncompensated magnetization at the FeF_2-Cu interface becomes pinned along a well-defined direction after field-cooling, and scattering of the electrons polarized by the Co layer by this pinned magnetization produces the GMR [Fig. 1(a)]. When the valve is rotated, the magnetization in the Co layer [red arrow in Fig. 1(c and d)] remains aligned along H_{meas}, while the pinned magnetization rotates with the valve [blue arrow in Fig. 1(c and d)].

The GMR depends on the mutual orientation of the magnetization in the Co layer and the pinned magnetization at the FeF_2-Cu interface. The GMR reaches its extrema when these magnetizations are collinear (i.e., parallel or antiparallel). The experimental angular dependences of the resistance are fitted to Eq. (1), which contains the term describing the *normal* GMR. The *normal* GMR implies that the valve's resistance reaches maximum and minimum values when the magnetizations in the Co layer and at the FeF_2-Cu interface are antiparallel and parallel, respectively. However, since FeF_2 and Co are dissimilar materials, an *inverse* GMR may be realized in the FeF_2/Cu/Co valves. In this case, the resistance maximum and minimum occur when the magnetizations are parallel and antiparallel, respectively. Determining the type of the GMR effect realized in the AFSVs requires calculations of a spin-polarized electronic band structure which goes beyond the scope of this work. Therefore, we assume that θ_{pin} obtained from a fit to Eq. (1) determines only the axis along which the magnetization is pinned but not its sign (direction along that axis). However, since the sign of the GMR remains the same for different measurements of the same system, the GMR is sensitive to the reversal of the pinned magnetization by 180º.

B. Field cooling and the anisotropy of the boundary magnetization

If the valve is cooled in a magnetic field along the easy axis (θ_{cool} = 0º or 180º), $\theta_{pin} = \theta_{cool}$ + 180º (assuming the *normal* GMR) or $\theta_{pin} = \theta_{cool}$ (assuming *inverse* GMR). Hence, for cooling along the easy axis, the pinned uncompensated magnetization at the FeF_2-Cu interface aligns parallel to the cooling field axis. The observation of finite ΔR_{GMR} even in H_{meas} = 90 kOe [Fig. 1(c)] indicates that pinning is unusually strong. On the other hand, when the AFSV is cooled in zero field, the GMR signal is

zero, which implies that the pinned uncompensated magnetization in that case is randomly distributed in both directions along the FeF_2 easy axis [schematics in Fig. 1(d)].

The angular dependence of the resistance measured after cooling the valve in the 90-kOe magnetic field applied perpendicular to the easy axis [Fig. 4(a)] demonstrates another unusual aspect of this pinning. Although the valve was cooled in a very strong magnetic field (90 kOe), the interfacial FeF_2-Cu magnetization is pinned perpendicular to the cooling field and parallel to the easy axis. The reason for this is that the magnetic field cannot be aligned perfectly perpendicular to the easy axis, i.e., it always has a finite projection along this axis, and the pinned magnetization aligns in the direction of this projection. Since $\theta_{pin} = 180^o$ (assuming *normal* GMR) for the nominal $\theta_{cool} = 90^o$ [Fig. 4(a)], the easy axis is slightly rotated anticlockwise with respect to the long edge of the AFSV, as shown in the schematic in Fig. 4(a). Therefore, if θ_{cool} is decreased, θ_{pin} should remain at 180º. On the other hand, at a certain orientation where θ_{cool} is greater than 90º, the cooling field projection along the easy axis should change sign which would reverse the pinned magnetization, i.e., θ_{pin} should switch from 180º to 0º. These expectations are confirmed by the angular dependences of the resistance shown in Fig. 4(b and c), which clearly show that θ_{pin} is 180º and 0º for $\theta_{cool} = 70^o$ and $\theta_{cool} = 110^o$, respectively. Thus, we concluded that, at low temperatures, the magnetization at the FeF_2(110)/Cu interface is always pinned along the easy axis, and its direction is determined by the projection of the cooling field on the easy axis. This is similar to the observations made by Olamit et al. [19,20] for an exchange bias bilayer system FeF_2/Co.

The large anisotropy in FeF_2 is responsible for the direction in which the surface magnetization is pinned upon field cooling. However, in general, an uncompensated surface magnetization anisotropy could be different from that in the bulk of an antiferromagnet. The fact that the two anisotropies coincide is an additional proof of the strong coupling of the surface uncompensated magnetization with the bulk antiferromagnetic order parameter, which, in turn, is an additional indirect confirmation for the proposed mechanism of the origin of the uncompensated magnetization at the [110] surface of FeF_2.

C. Origin of the macroscopic boundary magnetization in FeF_2 from the symmetry analysis

Symmetry considerations give further insight into the observed behavior. To determine whether a given interface of FeF_2 has an equilibrium magnetization, we need to identify the subgroup of its bulk magnetic point group $4'/mm'm$ that leaves the normal vector of the given surface invariant and determine whether this subgroup is compatible with ferromagnetism, i.e., whether it allows an invariant axial vector [14]. These subgroups are determined by inspection: $4'm'm$ for the (001) surface, $mm2$ for (100), and $m'm2'$ for (110). Of these groups, only $m'm2'$ is compatible with ferromagnetism. Thus, on a macroscopic scale, the (110) surface of FeF_2 has a net magnetization, whereas the (001) and (100) surfaces are fully compensated. This

analysis shows that, for the FeF_2(110) layer, the uncompensated surface magnetization is preserved even if the surface is not atomically flat. In contrast, for the (001) and (100) FeF_2 layers, surface roughness causes the interface magnetization to be zero [14]. These results are very unusual since they are opposite to the conclusions which could be made by looking at a perfect FeF_2 spin lattice. In that approach, for single domain FeF_2 crystals with perfectly smooth surfaces [(110), (100), and (001)] (see Fig. 1 in Ref. [4], for example), the (100) and (001) surfaces are magnetically uncompensated, whereas the (110) surface is nominally compensated.

Furthermore, the $m'm2'$ subgroup of the (110) surface contains no elements that interchange the two magnetic sublattices in FeF_2. Therefore, the equivalence of the two sublattices is broken at the (110) interface; the resulting boundary magnetization is not a relativistic effect and is generally expected to be large [14]. Inequivalence of the magnetic sublattices at the (110) surface can be understood in simple terms by inspecting the magnetic structure of the crystal in a single-domain state with a surface that has atomic steps, as schematically shown in Fig. 5. The two magnetic sublattices are shown using green (sublattice 1) and orange (sublattice 2) arrows pointing in and out of the page. All Fe atoms in sublattice 1 are bonded with F atoms above and below, whereas those in sublattice 2 with F atoms in front and in the back. While these bonds are equivalent in the bulk, they are crystallographically distinct near the surface, and thus the near-surface Fe atoms in sublattices 1 and 2 are in different chemical environments [21]. Generally speaking, these atoms may have different magnetic moments [22]. Moreover, their chemical inequivalence is likely to result in a surface termination with a preferred exposure of one sublattice to the surface and to the Cu atoms in the neighboring layer, yielding a net magnetization at the surface. Thus, macroscopically the (110) surface of FeF_2 has a net magnetization, which is responsible for the observed GMR.

Vanishing of the GMR measured in the 90-kOe magnetic field above the bulk FeF_2 Néel temperature (78 K) (Fig. 2) confirms that the GMR signal is related to the antiferromagnetic order in FeF_2. The uncompensated magnetization at the FeF_2(110)/Cu interface arises from the same magnetic moments that constitute the antiferromagnetic spin lattice, and, hence it is linearly exchange coupled [13,14] to the bulk FeF_2 antiferromagnetic order parameter. This yields a strong pinning of the boundary magnetization along the direction of the bulk easy axis. The magnetic field couples to the boundary magnetization and thereby to the bulk antiferromagnetic order parameter. Therefore, field cooling creates a preference for one of the two antiferromagnetic domains in FeF_2 and imposes the direction of the pinned magnetization. Once the AFSV is cooled below the Néel temperature, the boundary magnetization is "frozen in" and the external field can no longer reorient it. This explains why, at 10 K, the pinned magnetization aligns parallel to the FeF_2 easy axis regardless of the orientation of the cooling field. In order to permanently reverse this boundary magnetization after field cooling, an entire antiferromagnetic domain must be switched,

whereas the Zeeman coupling is only present at the surface. Since FeF_2 has a large uniaxial anisotropy, this reversal requires a very strong magnetic field at low temperatures. If the FeF_2 layer is sufficiently thick, Zeeman coupling at the surface becomes ineffective, and switching may only occur through the bulk spin-flop transition. This explains why the GMR signal measured at 10 K remains unchanged as H_{meas} is varied from 5 to 90 kOe [Fig. 3(a)].

D. Isothermal reversal of the pinned boundary magnetization

The fact that the GMR measured at 10 K remains the same in the entire H_{meas} range confirms the unprecedented stability of the pinned magnetization at low temperatures. At the same time, the suppression of the GMR signal by a strong magnetic field at 65 and 70 K [Fig. 3(a)] indicates that such fields affect the microscopic spin structure of FeF_2 in the vicinity of the paramagnetic transition. In particular, this explains the abrupt drop near 60 K in the temperature dependence of GMR (Fig. 2), and vanishing signal above the critical field of 80 kOe (55 kOe) at 65 K (70 K) in the field dependences of GMR [Fig. 3(a)]. Two microscopic mechanisms of the boundary magnetization reversal can be envisioned. First, due to reduction of anisotropy, the boundary magnetization may tend to align parallel to the external magnetic field, thereby remaining parallel to the Co-layer magnetization, which would result in the absence of the GMR signal. Second, close to the Néel temperature of FeF_2, the external field below 90 kOe may induce either a spin-flop transition or a transition to a paramagnetic state [23-25]. As a result, either the boundary magnetization and the bulk antiferromagnetic order parameter would align perpendicular to the external field, or the antiferromagnetic order would disappear, respectively. In both cases, the boundary magnetization would rotate in unison with the external magnetic field. This, in turn, would yield the absence of the GMR signal.

According to Fig. 3(a), if the AFSV is oriented at θ_{cool} while H_{meas} is changed, then pinning is completely restored in low magnetic fields. Thus, the ramp-up and ramp-down branches almost coincide for 65-K and 70-K curves in Fig. 3(a). This means that pinning can be erased and restored isothermally, slightly below the Néel temperature, without repeating the cooling procedure. Moreover, the angular dependence of the resistance is almost unchanged after application of a 50-kOe magnetic field [Fig. 3(b and c)]. In contrast, the minimum of the resistance shifts by 180º after subjecting the valve to magnetic field of 70 kOe [Fig. 3(d)]. These observations can be interpreted as follows. Since 50 kOe is below the GMR suppression field at 70 K, applying this field in the direction opposite to the cooling field does not affect the pinned magnetization at the FeF_2 interface. In contrast, the 70-kOe magnetic field applied opposite to the cooling field reverses the pinned boundary magnetization, which is subsequently pinned when the magnetic field is ramped down to 10 kOe [Fig. 3(d)]. Overall, these measurements demonstrate that, at temperatures slightly below the Néel temperature, the pinned magnetization at the boundary of FeF_2 may be reversed by applying a sufficiently strong magnetic field. Such reversal of the boundary magnetization in a strong magnetic field at temperatures close to the Néel temperature may be employed for isothermal imprinting of pinning.

E. Further considerations

Since the pinned uncompensated magnetization can induce the exchange bias, many phenomena observed in FeF_2/Cu /Co spin valves are directly relevant to the phenomena observed in bilayers composed of epitaxial FeF_2 and ferromagnetic layers. First, strong exchange bias has been observed in FeF_2(110)/ferromagnet bilayers, whereas the exchange bias in FeF_2(100)/ferromagnet and FeF_2(001)/ferromagnet bilayers is weak [4]. Second, in Ref. [26], it was shown that applying a high magnetic field at temperatures slightly below the Néel temperature strongly affects the exchange bias field in MnF_2/Fe bilayers. Similarly to the FeF_2(110)/Cu/Co valve, the effect emerges due to the reversal of the antiferromagnetic spin structure in the vicinity of a paramagnetic phase [25]. Third, in FeF_2(110)/Co bilayers, strong pining of the boundary magnetization along the FeF_2 easy [001] axis was found to be dependent only on the projection of the cooling field on the easy axis, and not on the cooling field direction [20]. Finally, our observations suggest that, at temperatures close to the Néel temperature of FeF_2, exchange bias may be imprinted isothermally in a FeF_2(110)/ferromagnet bilayer by applying magnetic field strong enough to overcome the anisotropy of FeF_2.

A series of experiments demonstrated that defects inside the FeF_2 layer and at its interface strongly influences the exchange bias, and hence magnetization pinning, in the FeF_2/ferromagnet bilayers [27-29]. Such defects may be pinned after field cooling and contribute to GMR. It is impossible to exclude the role of the defects on the GMR in the FeF_2(110)/Cu/Co AFSV, and that these defects might also be pinned after field cooling. For this case, it is hard to predict the relative strength their contribution to the observed GMR. Moreover, it might be difficult to separate it from the contribution by the mechanism proposed above. However, the symmetry mechanism proposed in this work is intrinsic and is not affected by defects. Moreover, the general properties of the boundary magnetization following from symmetry also apply to defects located near the surface. It is important that the symmetry mechanism yields a robust explanation for the dependence of uncompensated surface magnetization on crystalline orientation of the FeF_2 layer.

We should point out that the AFSV technique was previously used to detect the strongly pinned uncompensated magnetization at the FeMn-Cu interface [11]. There are two important differences between those devices and the AFSV studied here. First, the FeMn layer in Ref. [11] was polycrystalline, whereas the FeF_2 layer is epitaxial, which allowed us to study FeF_2-based valves with different crystallographic orientations. This analysis leads to a clear conclusion on the relationship between the crystallographic symmetry and magnetization of the interface. Second, the fact that FeF_2 is an insulator allows us to connect directly the behavior of the magnetoresistance to the FeF_2-Cu interfacial magnetization.

V. CONCLUSION

Sensitive magnetotransport measurements of AFSVs containing an epitaxial FeF_2 layer confirm the presence of pinned uncompensated magnetization at the FeF_2(110)/Cu interface, as expected from symmetry considerations. Due to strong coupling of this uncompensated magnetization to the staggered bulk FeF_2 spin structure, which has high anisotropy, this magnetization is unusually stable below the Néel temperature (78 K). Specifically, a magnetic field as high as 90-kOe has no effect on the pinning at 10 K. Close to the Néel temperature, the anisotropy of FeF_2 anisotropy is reduced, and the reversal of the interfacial magnetization becomes possible. This effect can be used for isothermal imprinting of the boundary magnetization.

FeF_2 is the second insulating antiferromagnet, after Cr_2O_3 [16], in which the surface magnetization was confirmed experimentally. In contrast, the presence of time-reversal symmetry forbids roughness-insensitive boundary magnetization in NiO and CoO. The AFSV technique developed here can also be used to probe the surface magnetization in metallic CuMnAs and Mn_2Au antiferromagnets whose spin structures can be manipulated electrically [30,31]. The absence of a macroscopic time-reversal symmetry in those materials implies that their (001) surfaces must have a surface magnetization coupled to the bulk antiferromagnetic order parameter, similar to the FeF_2(110) surface considered here. We emphasize that the GMR technique can be used to detect 180-degree switching of the antiferromagnetic order parameter. This aspect may make this detection method attractive for applications in antiferromagnetic memory devices.

ACKNOWLEDGEMENTS

This work was supported by the Office of Basic Energy Science, U.S. Department of Energy, BES-DMS funded by the Department of Energy's Office of Basic Energy Science, DMR under grant DE FG02 87ER-45332. K.B. is supported by the NSF through Grants No. DMR-1609776, No. DMR-1916275, and Nebraska Materials Research Science and Engineering Center (MRSEC) Grant No. DMR-1420645.

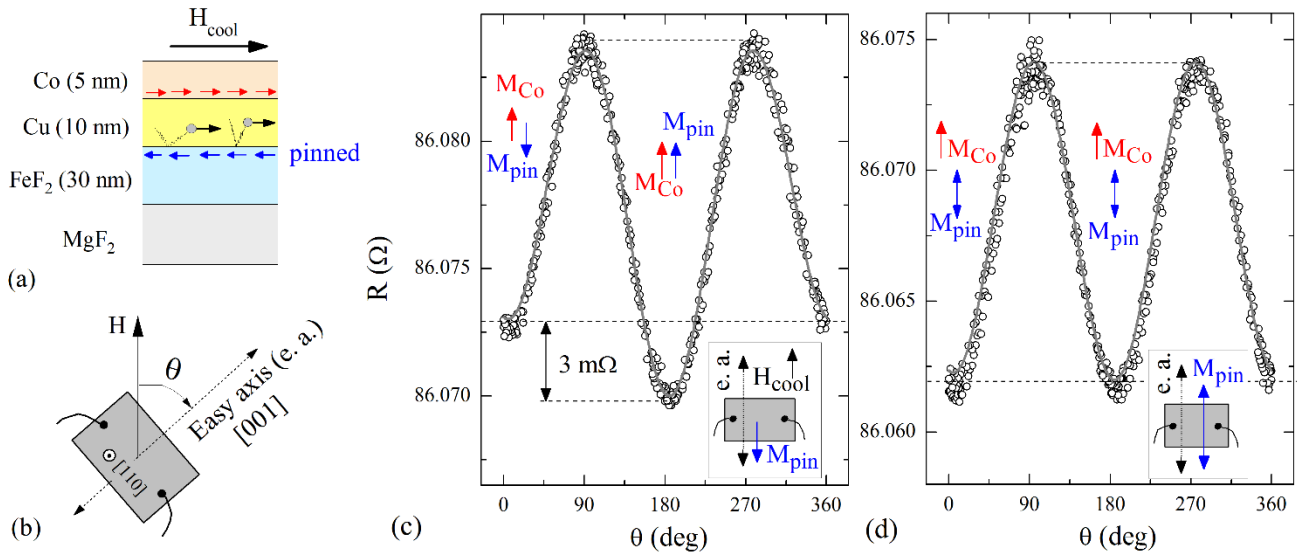

FIG. 1 (a) Schematics illustrates scattering of electrons polarized by the Co layer on the pinned uncompensated magnetization at the FeF_2-Cu interface. (b) Schematics shows rotation of the FeF_2(110)/Cu/Co valve in an external magnetic field; easy axis (e. a.) is perpendicular to the long edge of the sample, the sample orientation is defined by an angle θ between the direction of magnetic field and the easy axis. Angular dependences of resistance, R, for the FeF_2(110)/Cu/Co AFSV measured at 10 K in a 90-kOe magnetic field after cooling the valve from 300 K (c) in the 90-kOe magnetic field applied along the easy axis of FeF_2 ($\theta_{cool} = 0°$), (d) after cooling in zero magnetic field (ZFC). Circles show experimental data, grey lines are the fits to Eq. (1). Blue and red arrows show the orientation of the pinned uncompensated magnetization (M_{pin}) at the FeF_2-Cu interface (assuming the *normal* GMR) and the Co layer (M_{Co}), respectively. The schematics in the boxes at (c, d) illustrate the mutual orientation of cooling magnetic field (H_{cool}), M_{pin}, and the FeF_2 easy axis for the particular field-cooling procedures.

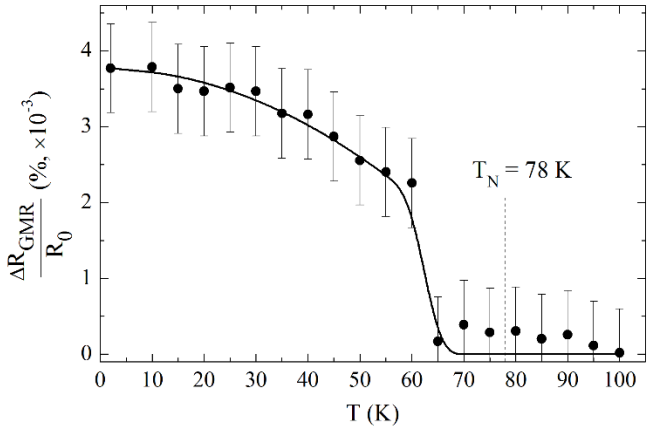

FIG. 2 Temperature dependence of GMR for the FeF_2(110)/Cu/Co AFSV measured in a 90-kOe magnetic field after cooling the valve in a 90-kOe magnetic field. The dashed vertical line shows the Néel temperature of bulk FeF_2. The black curve is a guide to the eye.

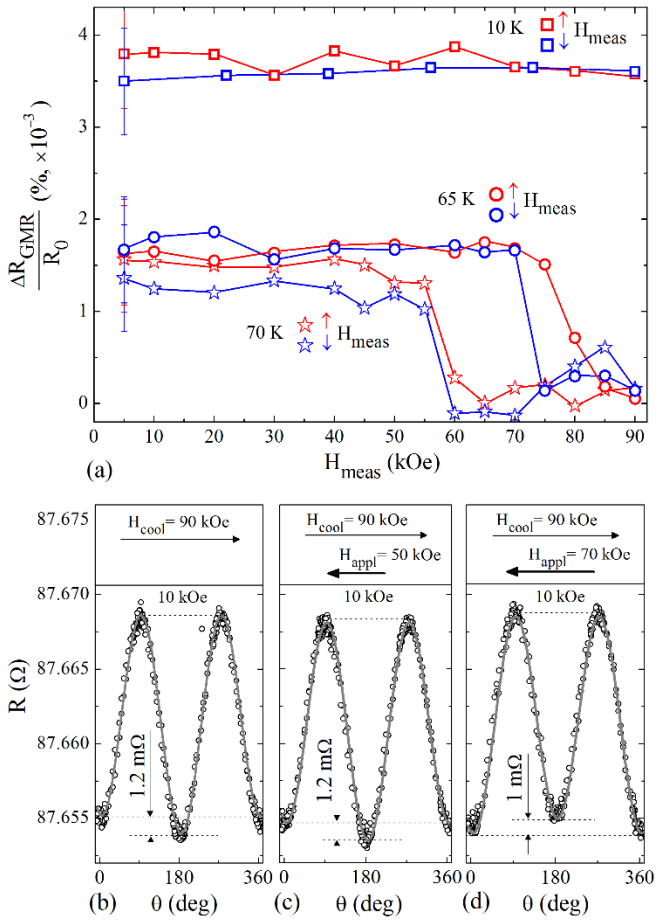

FIG. 3 (a) Magnetic-field dependences of GMR measured at 10 K (rectangles), 65 K (circles), and 70 K (stars). The data were obtained by cooling the valve to the corresponding temperature in a 90-kOe magnetic field and sequentially measuring the angular dependence incrementally ramping up H_{meas} (red curves) and then down (blue curves). The error bars in (a) are shown only for a 5-kOe data point. (b) Angular dependences of resistance measured at 70 K in a 10-kOe magnetic field after cooling the FeF_2(110)/Cu/Co AFSV in the 90-kOe magnetic field applied along the easy axis of FeF_2 (θ_{cool} = 0º); the same dependences measured in the 10-kOe magnetic field after applying (c) 50-kOe and (d) 70-kOe magnetic field (H_{appl}) in the direction opposite to the cooling field (H_{cool}). In (b-d), circles are experimental data, grey lines are the fits to Eq. (1).

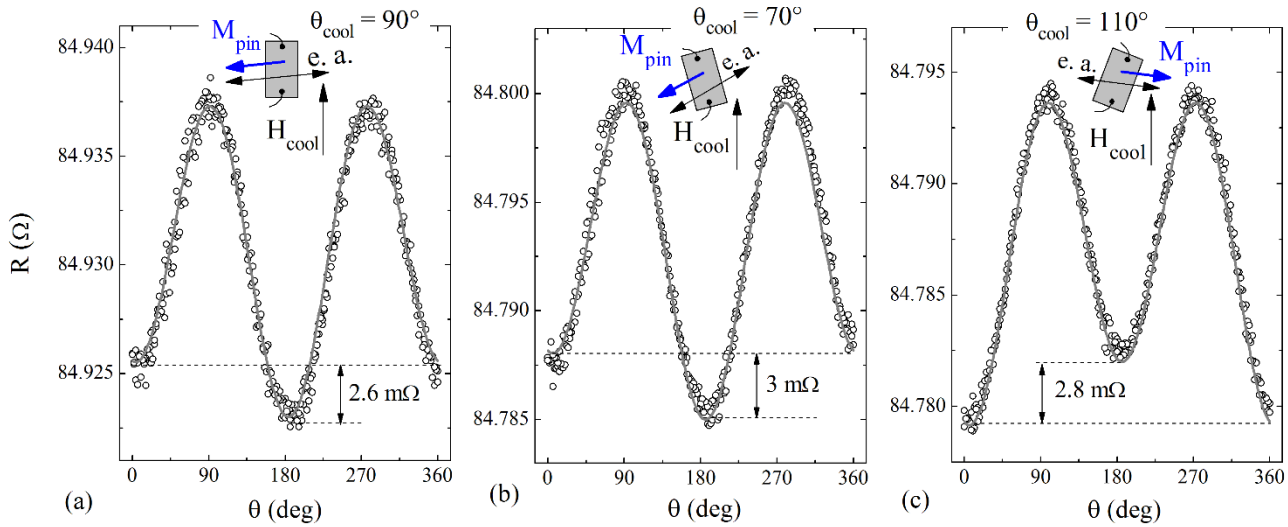

FIG. 4 Angular dependences of resistance for the FeF_2(110)/Cu/Co AFSV measured at 10 K in a 90-kOe magnetic field after cooling the valve from 300 K in the 90-kOe magnetic field while sample orientations are (a) θ_{cool} = 90º, (b) θ_{cool} = 70º, (c) θ_{cool} = 110º. Circles are experimental data, grey lines are the fits to Eq. (1). The schematics at top of each plot illustrate the mutual orientation of the easy axis (e. a.) and the pinned magnetization (M_{pin}) (assuming the *normal* GMR) with respect to the cooling field (H_{cool}) direction. Schematic at top corner at (a) explicitly illustrates that the easy axis is not completely perpendicular to the long edge of the sample, consequently, a projection of H_{cool} on the easy axis defines the direction of the pinned magnetization.

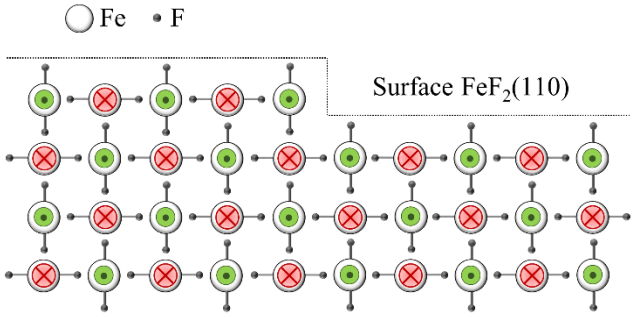

FIG. 5 Schematics illustrates the crystallographic and spin structures of the $FeF_2(110)$ layer with an atomic step. The green and red circles depict the Fe spins pointed in and out of the page, respectively, along the easy axis of FeF_2.

REFERENCES

[1] V. Baltz, A. Manchon, M. Tsoi, T. Moriyama, T. Ono, and Y. Tserkovnyak, Rev. Mod. Phys. **90**, 015005 (2018).
[2] K. Olejník, T. Seifert, Z. Kašpar, V. Novák, P. Wadley, R. P. Campion, M. Baumgartner, P. Gambardella, P. Němec, J. Wunderlich, J. Sinova, P. Kužel, M. Müller, T. Kampfrath, and T. Jungwirth, Sci. Adv. **4**, eaar3566 (2018).
[3] R. Cheng, D. Xiao, and A. Brataas, Phys. Rev. Lett. **116**, 207603 (2016).
[4] J. Nogués, T. J. Moran, D. Lederman, I. K. Schuller, and K. V. Rao, Phys. Rev. B **59**, 6984 (1999).
[5] C. Tsang, N. Heiman, and K. Lee, J. Appl. Phys. **52**, 2471 (1981).
[6] M. J. Carey and A. E. Berkowitz, Appl. Phy. Lett. **60**, 3060 (1992).
[7] R. Jungblut, R. Coehoorn, M. T. Johnson, Ch. Sauer, P. J. van der Zaag, A. R. Ball, Th. G. S. M. Rijks, J. aan de Stegge, and A. Reinders, J. Magn. Magn. Mater. **148**, 300 (1995).
[8] P. J. van der Zaag, A. R. Ball, L. F. Feiner, R. M. Wolf, and P. A. A. van der Heijden, J. Appl. Phys. **79**, 5103 (1996).
[9] H. Ohldag, A. Scholl, F. Nolting, E. Arenholz, S. Maat, A. T. Young, M. Carey, and J. Stöhr, Phys. Rev. Lett. **91**, 017203 (2003).
[10] J. Nogués and I. K. Schuller, J. Magn. Magn. Mater. **192**, 203 (1999).
[11] P. N. Lapa, I. V. Roshchin, J. Ding, J. E. Pearson, V. Novosad, J. S. Jiang, and A. Hoffmann, Phys. Rev. B **95**, 020409(R) (2017).
[12] B. G. Park, J. Wunderlich, X. Martí, V. Holý, Y. Kurosaki, M. Yamada, H. Yamamoto, A. Nishide, J. Hayakawa, H. Takahashi, A. B. Shick, and T. Jungwirth, Nat. Mater. **10**, 347 (2011).
[13] A. F. Andreev, JETP Lett. **63**, 758 (1996).
[14] K. D. Belashchenko, Phys. Rev. Lett. **105**, 147204 (2010).
[15] L. D. Landau, L. P. Pitaevskii, and E. M. Lifshits, *Electrodynamics of continuous media* (Butterworth-Heinemann, Oxford, 1984), Sec. 51.
[16] X. He, Y. Wang, N. Wu, A. N. Caruso, E. Vescovo, K. D. Belashchenko, P. A. Dowben, and C. Binek, Nat. Mater. **9**, 579 (2010).
[17] C. Hahn, G. de Loubens, V. V. Naletov, J. Ben Youssef, O. Klein, and M. Viret, Europhys. Lett. **108**, 57005 (2014).
[18] S. M. Rezende, R. L. Rodríguez-Suárez, and A. Azevedo, Phys. Rev. B **93**, 054412 (2016).
[19] J. Olamit, E. Arenholz, Z.-P. Li, O. Petracic, I. V. Roshchin, R. Morales, X. Batlle, I. K. Schuller, and K. Liu, Phys. Rev. B **72**, 012408 (2005).
[20] J. Olamit, Z.-P. Li, I. K. Schuller, and K. Liu, Phys. Rev. B **73**, 024413 (2006).
[21] S. López-Moreno, A. H. Romero, J. Mejía-López, A. Muñoz, and I. V. Roshchin, Phys. Rev. B **85**, 134110 (2012).
[22] D. Lederman, R. Ramírez, and M. Kiwi, Phys. Rev. B **70**, 184422 (2004).
[23] S. M. Rezende, J. Phys. C **11**, L701 (1978).
[24] V. Jaccarino, A. R. King, M. Motokawa, T. Sakakibara, and M. Date, J. Magn. Magn. Mater. **31-34**, 1117 (1983).
[25] Y. Shapira and S. Foner, Phys. Rev. B **1**, 3083 (1970).
[26] J. Nogués, L. Morellon, C. Leighton, M. R. Ibarra, and I. K. Schuller, Phys. Rev. B **61**, R6455 (2000).
[27] A. C. Basaran, T. Saerbeck, J. de la Venta, H. Huckfeldt, A. Ehresmann, and I. K. Schuller, Appl. Phy. Lett. **105**, 072403 (2014).
[28] J. Nogués, D. Lederman, T. J. Moran, I. K. Schuller, and K. V. Rao, Appl. Phy. Lett. **68**, 3186 (1996).
[29] F. Torres, R. Morales, I. K. Schuller, and M. Kiwi, Nanoscale **9**, 17074 (2017).
[30] P. Wadley, B. Howells, J. Železný, C. Andrews, V. Hills, R. P. Campion, V. Novák, K. Olejník, F. Maccherozzi, S. S. Dhesi, S. Y. Martin, T. Wagner, J. Wunderlich, F. Freimuth, Y. Mokrousov, J. Kuneš, J. S. Chauhan, M. J. Grzybowski, A. W. Rushforth, K. W. Edmonds, B. L. Gallagher, and T. Jungwirth, Science **351**, 587 (2016).
[31] I. A. Zhuravlev, A. Adhikari, and K. D. Belashchenko, Appl. Phy. Lett. **113**, 162404 (2018).